Interaction Notes
Note 404
1 December 1980

MULTI-SURFACE SHIELDED ENCLOSURES WITH PARTICULAR REFERENCE TO BONDING BETWEEN SHIELDS

K.S.H. Lee
The Dikewood Corporation
Santa Monica, California 90405

Abstract

This report extends the previous work on a single-surface shielded enclosure of arbitrary shape to a multi-surface enclosure with or without electrical bonding between the shields. It is found that the inductive mutual interactions among the shields and the bonding straps reduce the effectiveness of a multi-surface shielded enclosure against the penetration of external magnetic fields.

PREFACE

I would like to thank W.S. Kehrer, C.E. Baum, J.P. Castillo and K.C. Chen of the Air Force Weapons Laboratory for their interest and suggestions in this report. Sections V and VI were worked out in collaboration with F.C. Yang of Dikewood.

CONTENTS

ILLUSTRATIONS

ILLUSTRATIONS (Continued)

TABLES

I. INTRODUCTION

One of the most effective methods of protecting a system from undesirable EMP effects is by use of shielding. Although the basic principles of shielding for a single-surface enclosure are well understood (Ref. 1), the extension of these principles to multi-surface enclosures is by no means straightforward. Unique to multi-surface shielding is the mutual interaction among the shields, which may degrade the intended shielding performance of the enclosure. Another unique feature is the bonding that is often employed between the shields in order to reduce electrostatic hazards. This bonding practice may have an adverse effect on the protection of a shielded enclosure against magnetic-field penetration. The effects of shield-shield interaction and bonding will be treated in this report.

Figure 1 shows various topics that will be addressed in this report. In Section II, the problem of two concentric spherical shields will be solved using the theory of inductive shielding (Ref.1), and the results will be generalized to N-surface spherical shields. The corresponding results for cylindrical shields will be presented in Section III. Equivalent circuits will be constructed in Section IV to interpret the analytical results for a two-surface spherical enclosure; the results will be generalized to two-surface enclosures of arbitrary shape. In Section VI the effect of bonding on magnetic-field penetration into a two-surface enclosure will be discussed. Finally, the most important results are summarized in Section VII.

The underlying assumptions of inductive shielding are (1) the electric field is neglected everywhere except in the enclosure's wall where it is related to the induced current by Ohm's law, and (2) the wall thickness is much smaller than the typical linear dimension of the enclosure. In addition, this report assumes the wall thickness to be smaller than the wall's skin depth, except in Section V where this assumption is removed.

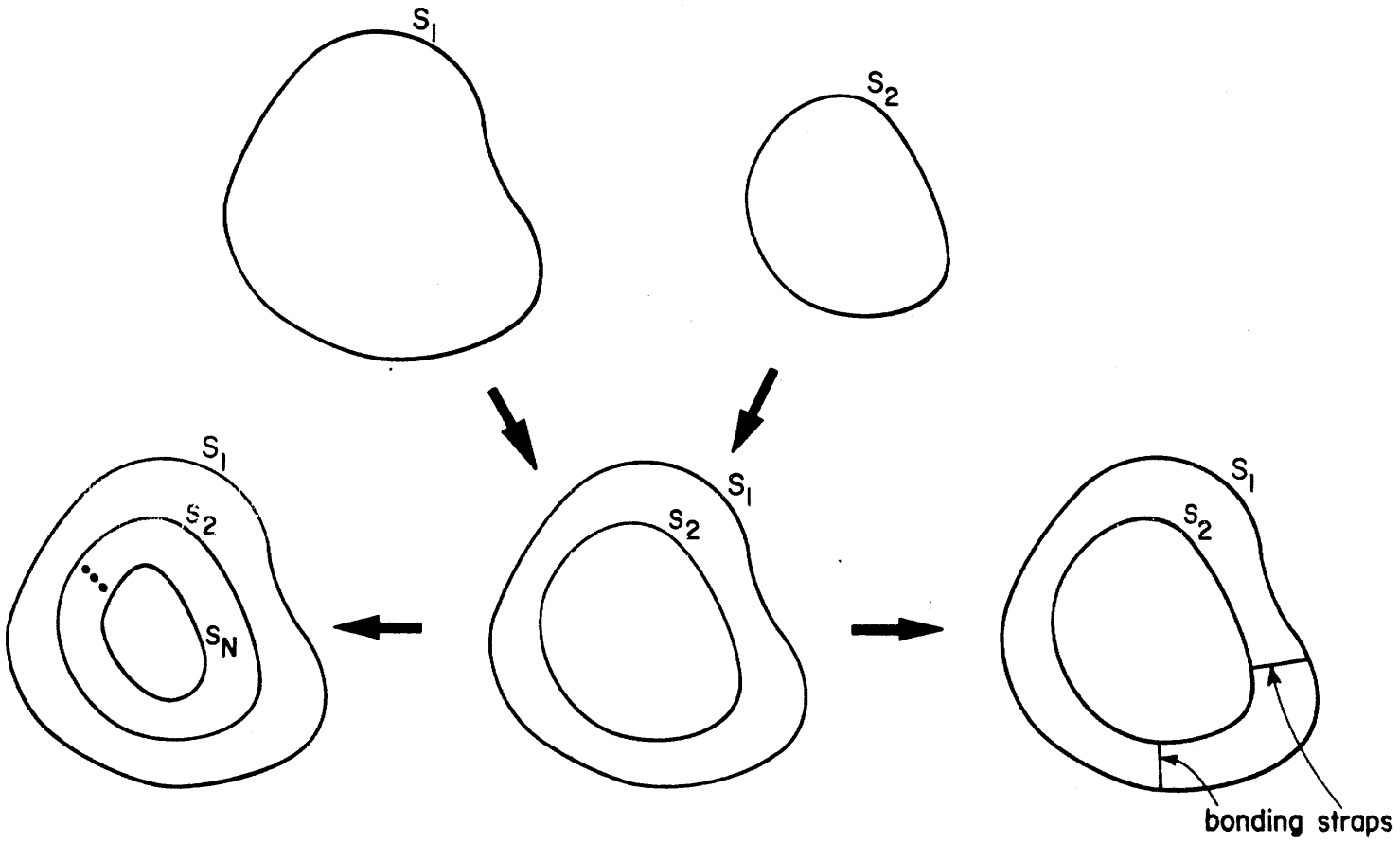

Figure 1. Problems for discussion.

II. SPHERICAL SHIELDS

In this section, the problem of two concentric spherical shells will first be treated with explicit simple engineering results given in frequency and time domains. The results for two shells will then be generalized to N concentric spherical shells. Discussions of equivalent circuits, generalization to shields of arbitrary shape, and effects of electrical bonding between the shells will be relegated to later sections.

1. TWO SPHERICAL SHIELDS

In Figure 2a is shown an enclosure with two concentric spherical shields immersed in a slowly varying magnetic field $H_o(t)$. Insofar as the penetrant field $H_i(t)$ is concerned, one may replace Figure 2a with Figure 2b with appropriate boundary conditions that duplicate the shielding properties of the walls (Ref. 1). The magnetic scalar potential Φ for the three regions shown in Figure 2b takes the form

$$\begin{aligned} \Phi_1 &= -\tilde{H}_o r\cos\theta + A\frac{a_1^3}{r^2}\cos\theta \qquad && r \geq a_1 \\ \Phi_2 &= B\,r\cos\theta + C\frac{a_1^3}{r^2}\cos\theta \qquad && a_1 \geq r \geq a_2 \\ \Phi_3 &= D\,r\cos\theta \qquad && r \leq a_2 \end{aligned} \tag{1}$$

where $\tilde{H}_o$ is the Laplace transform of $H_o(t)$. The constants A, B, C and D are determined by the following boundary conditions (Ref. 1 and Appendix A):

$$\begin{aligned} \frac{\partial}{\partial r}\Phi_1 &= \frac{\partial}{\partial r}\Phi_2, \qquad \text{at } r = a_1 \\ \frac{\partial}{\partial r}\Phi_2 &= \frac{\partial}{\partial r}\Phi_3, \qquad \text{at } r = a_2 \end{aligned} \tag{2}$$

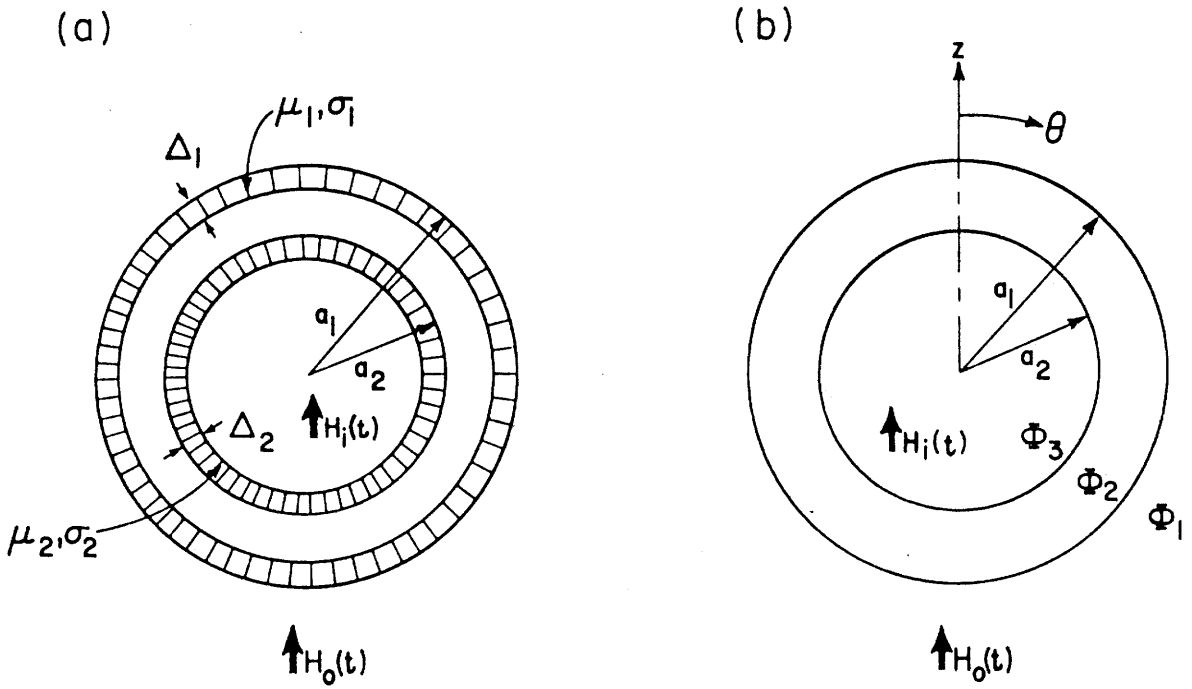

Figure 2. Two-surface spherical enclosure: (a) Two spherical shields in a slowly varying magnetic field; (b) Equivalent of (a) with appropriate boundary conditions.

$$\nabla_s^2 (\Phi_2 - \Phi_1) = s\mu_o \Delta_1 \sigma_1 \frac{\partial}{\partial r} \Phi_1, \qquad \text{at } r = a_1$$

$$\nabla_s^2 (\Phi_3 - \Phi_2) = s\mu_o \Delta_2 \sigma_2 \frac{\partial}{\partial r} \Phi_2, \qquad \text{at } r = a_2 \tag{3}$$

Equations 2 mean that the normal component of the magnetic field is continuous across the shield, while Equations 3 state that its tangential component is discontinuous by the amount of the current induced in the shield. From Equations 1 through 3 one finds that

$$\frac{\tilde{H}_i}{\tilde{H}_o} = \frac{1}{(1+\tau_1 s)(1+\tau_2 s) - (a_2/a_1)^3 \tau_1 \tau_2 s^2} \tag{4}$$

with

$$\tau_1 = \frac{1}{3} \mu_o a_1 \sigma_1 \Delta_1$$

$$\tau_2 = \frac{1}{3} \mu_o a_2 \sigma_2 \Delta_2 \tag{5}$$

If no interaction between the shields is assumed, Equation 4 becomes

$$\left.\frac{\tilde{H}_i}{\tilde{H}_o}\right|_{\text{no int}} = \frac{1}{(1+\tau_1 s)(1+\tau_2 s)} \tag{6}$$

as one would expect, since Equation 6 is the product of the transfer function of each individual shield. Equations 4 and 6 are plotted in Figure 3.

The time-domain solution of Equation 4 is

$$\frac{H_i(t)}{H_o} = \frac{1}{\sqrt{(\tau_1 - \tau_2)^2 + 4\tau_1 \tau_2 \alpha^3}} \left(e^{-t/T_1} - e^{-t/T_2} \right) \tag{7}$$

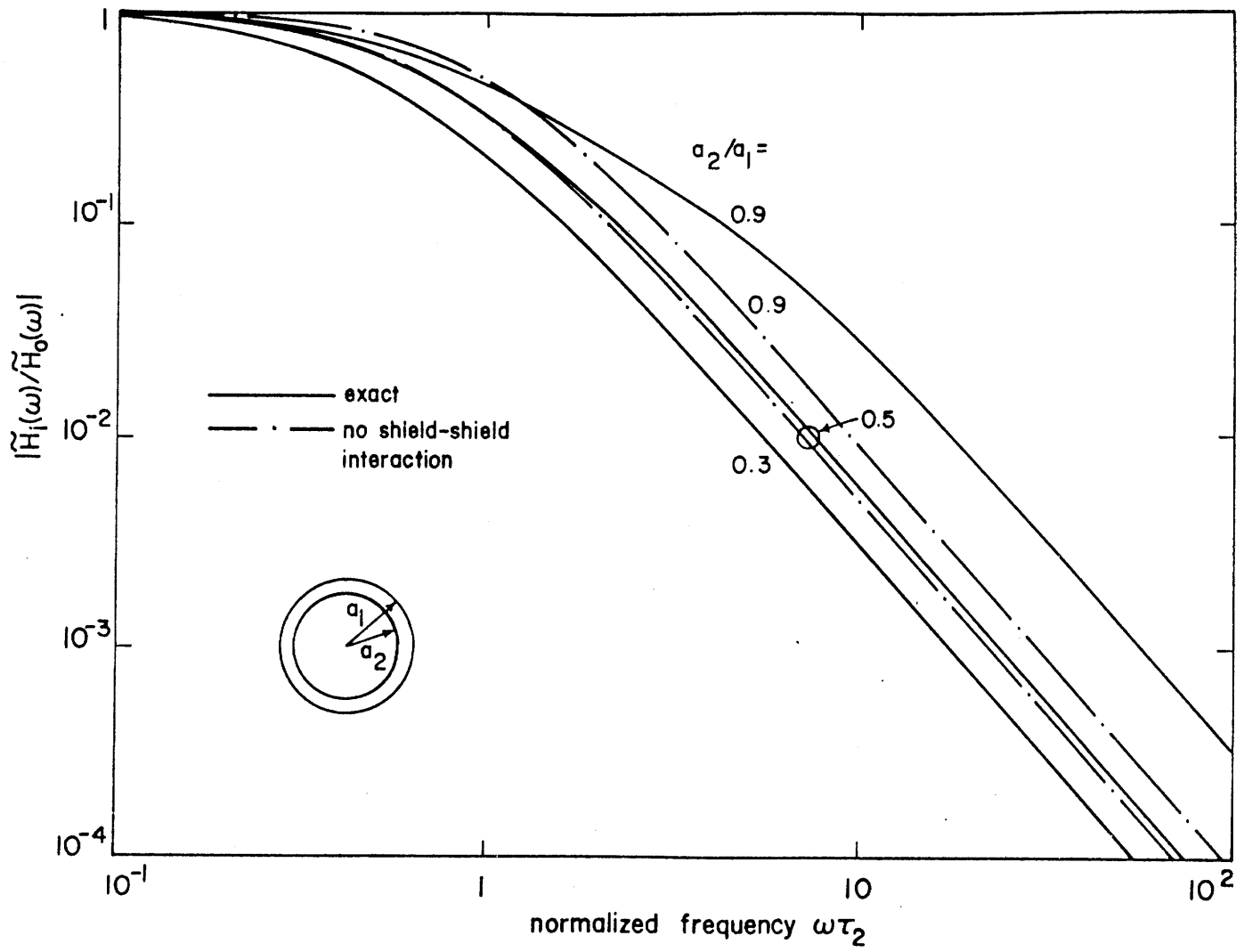

Figure 3. Frequency spectrum of the ratio $|\tilde{H}_i/\tilde{H}_o|$.

where

$$T_{1,2} = \frac{2\tau_1\tau_2(1-\alpha^3)}{\tau_1+\tau_2 \mp \sqrt{(\tau_1-\tau_2)^2 + 4\tau_1\tau_2\alpha^3}} \tag{8}$$

and $\alpha = a_2/a_1$, while the time-domain solution of Equation 6 is

$$\left.\frac{H_i(t)}{H_o}\right|_{\text{no int}} = \frac{1}{\tau_1-\tau_2}\left(e^{-t/\tau_1} - e^{-t/\tau_2}\right) \tag{9}$$

Here, H_o is the impulse strength of the external fields, and for most applications can be taken to be the time-integral of the magnetic field of a typical high-altitude EMP (Ref. 1).

Equations 7 and 9 are plotted in Figure 4 where one may see that for the case $a_2/a_1 = 0.9$, the neglect of shield-shield interaction amounts to 20% underestimate of the penetrant field.

From the viewpoint of the EMP hardness designer the currents induced in each enclosure's shield are important, since they are the only means to prevent the external field from penetrating into the interior of the enclosure. Let $\tilde{K}_{1\phi}$ and $\tilde{K}_{2\phi}$ denote the induced sheet currents in first and second shields of Figure 2. Then, from Equations 1 through 3 one obtains

$$\tilde{K}_{1\phi} = \frac{1}{a_1}\frac{\partial\Phi_2}{\partial\theta} - \frac{1}{a_1}\frac{\partial\Phi_1}{\partial\theta} \qquad (\text{at } r = a_1)$$

$$= -\frac{3}{2}\tilde{H}_o \frac{\tau_1 s(1+\tau_2 s) - \alpha^3\tau_1\tau_2 s^2}{(1+\tau_1 s)(1+\tau_2 s) - \alpha^3\tau_1\tau_2 s^2}\sin\theta \tag{10}$$

$$\tilde{K}_{2\phi} = \frac{1}{a_2}\frac{\partial\Phi_3}{\partial\theta} - \frac{1}{a_2}\frac{\partial\Phi_2}{\partial\theta} \qquad (\text{at } r = a_2)$$

$$= -\frac{3}{2}\tilde{H}_o \frac{\tau_2 s}{(1+\tau_1 s)(1+\tau_2 s) - \alpha^3\tau_1\tau_2 s^2}\sin\theta \tag{11}$$

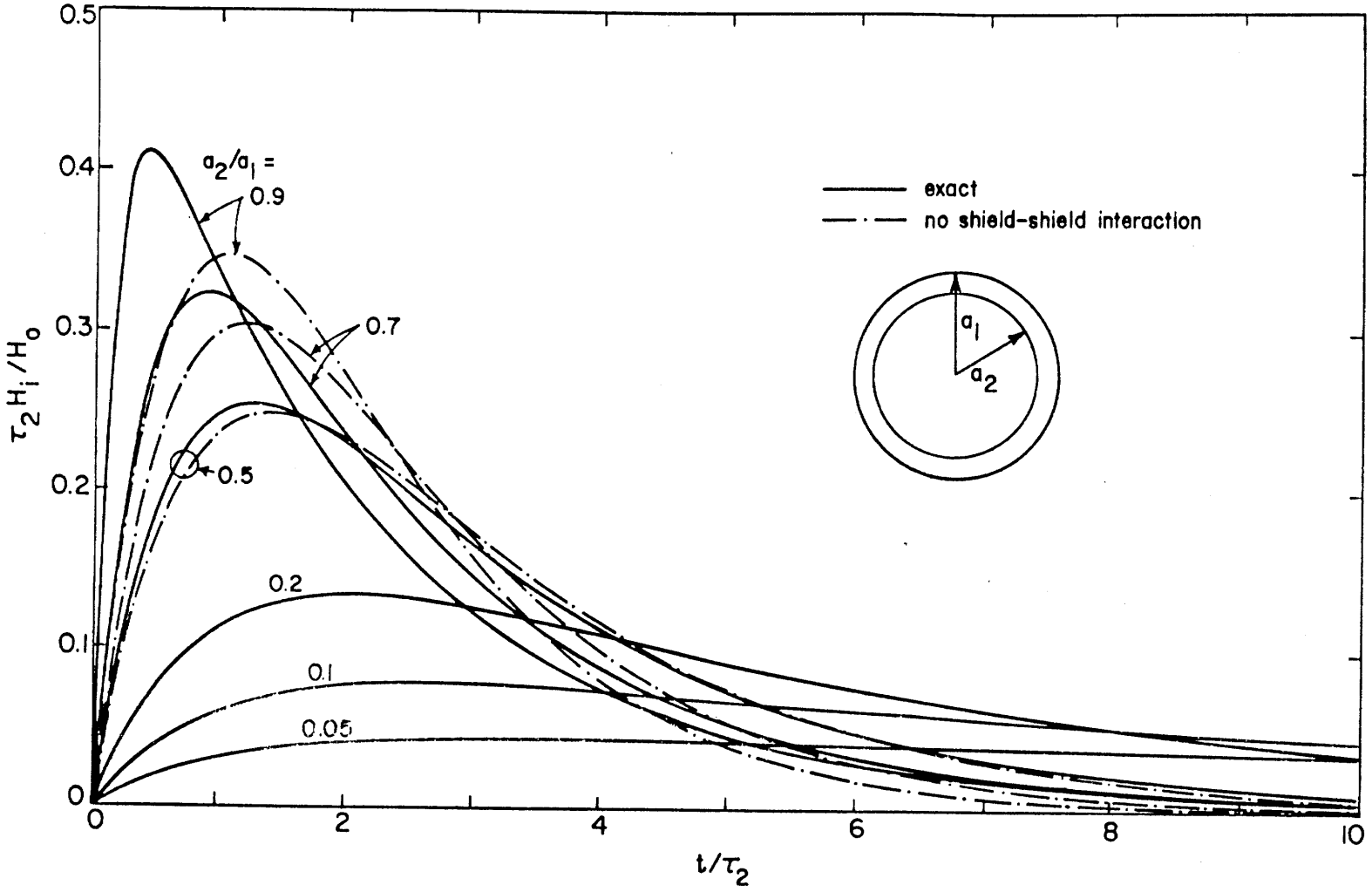

Figure 4. Time behavior of the penetrant field for an impulse external field.

These expressions for the currents will give a clue to construct equivalent circuits in Section IV.

2. N SPHERICAL SHIELDS

Let $\tilde{H}_i^{(2)}$, $\tilde{H}_i^{(3)}$, ... $\tilde{H}_i^{(N)}$ denote, respectively, the field that penetrates into a two-surface, three-surface, ... N-surface spherical enclosure.

For a two-surface enclosure Equation 4 gives

$$\tilde{H}_o/\tilde{H}_i^{(2)} = (1+\tau_1 s)(1+\tau_2 s) - \left(\frac{a_2}{a_1}\right)^3 \tau_1\tau_2 s^2$$

$$= 1 + (\tau_1+\tau_2)s + \left[1 - (a_2/a_1)^3\right]\tau_1\tau_2 s^2 \qquad (12)$$

For a three-surface shielded enclosure (Fig. 5a) one uses the same, although more complicated, procedure for the two-surface enclosure and finds

$$\tilde{H}_o/\tilde{H}_i^{(3)} = 1 + (\tau_1+\tau_2+\tau_3)s + \left[1 - (a_2/a_1)^3\right]\tau_1\tau_2 s^2 + \left[1 - (a_3/a_2)^3\right]\tau_2\tau_3 s^2$$

$$+\left[1 - (a_3/a_1)^3\right]\tau_3\tau_1 s^2 + \left[1 - (a_2/a_1)^3\right]\left[1 - (a_3/a_2)^3\right]\tau_1\tau_2\tau_3 s^2 \qquad (13)$$

The poles of $\tilde{H}_i(s)$ in the complex s-plane for two and three spherical shields are given in Table 1. These poles will immediately enable one to plot the frequency spectrum of the penetrant field, since they are the "break points" in the log-log scale plot (Fig. 6). From the table it is clear that as the second and/or the third shield get closer to the outer shield, the pole corresponding to the outermost shield moves toward the $j\omega$-axis away from its unperturbed value -1, while the pole corresponding to the second (third) shield (the second (third) column of Table 1) moves away from its unperturbed value $-1/\alpha$ ($-1/\alpha^2$) further away from the $j\omega$-axis.

For an N-surface spherical enclosure (Fig. 5b) one can write down, on a close examination of Equations 12 and 13,

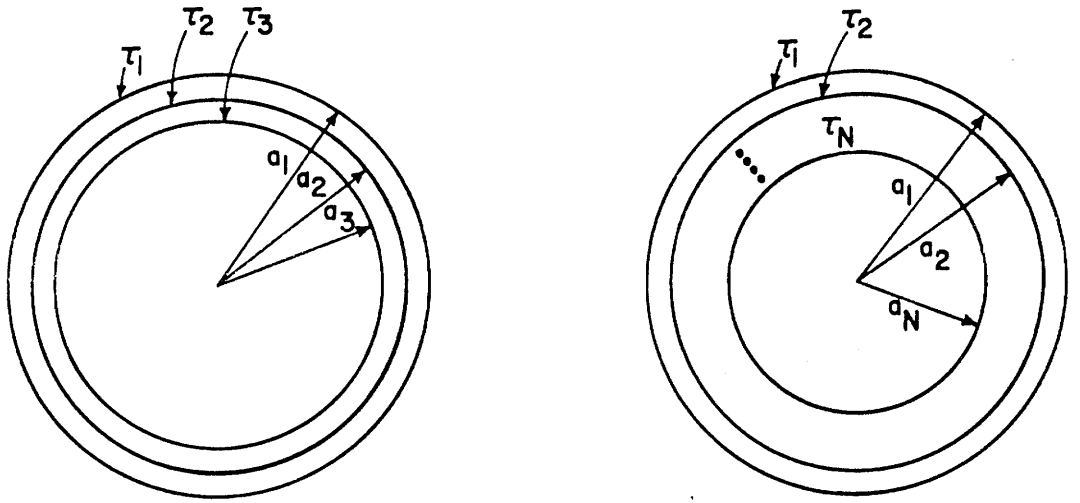

(a) Three-surface spherical enclosure

(b) N-surface spherical enclosure

Figure 5. Multi-surface spherical shields.

TABLE 1. s-PLANE POLES FOR TWO-SURFACE AND THREE-SURFACE SPHERICAL ENCLOSURES. THE VALUES ARE FOR $\bar{s} = \tau_1 s$ WITH $\alpha = a_2/a_1 = a_3/a_2$ AND $\tau_2/\tau_1 = \tau_3/\tau_2 = \alpha$

α	Two Shields		Three Shields		
	$\bar{s}_1$	$\bar{s}_2$	$\bar{s}_1$	$\bar{s}_2$	$\bar{s}_3$
0.1	- 1.00	-10.01	- 1.00	-10.01	-100.11
0.2	- 1.00	- 5.05	- 1.00	- 5.04	- 25.25
0.3	- 0.99	- 3.46	- 0.99	- 3.43	- 11.55
0.4	- 0.96	- 2.77	- 0.96	- 2.67	- 6.96
0.5	- 0.91	- 2.52	- 0.90	- 2.29	- 5.10
0.6	- 0.83	- 2.57	- 0.79	- 2.13	- 4.49
0.7	- 0.73	- 2.96	- 0.66	- 2.17	- 4.72
0.8	- 0.65	- 3.96	- 0.53	- 2.56	- 6.03
0.9	- 0.57	- 7.22	- 0.42	- 4.10	- 10.81

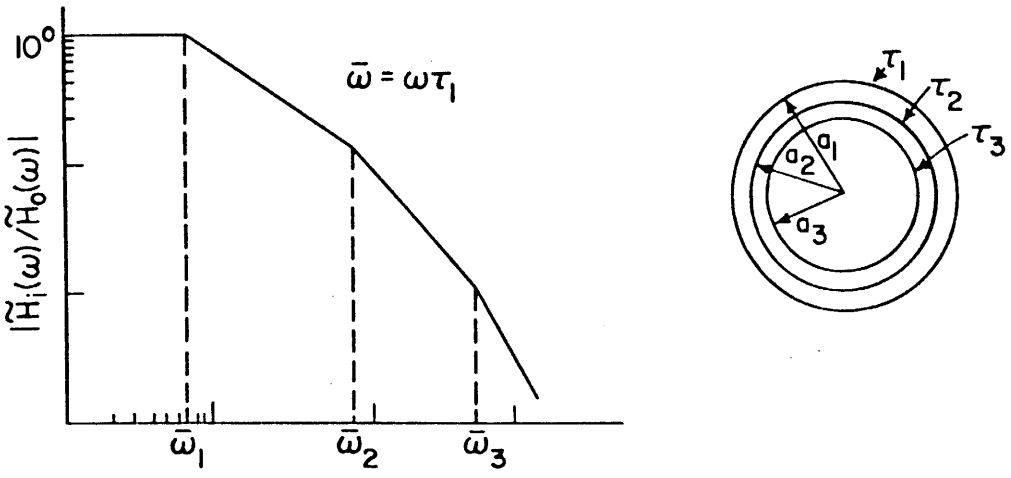

Figure 6. Frequency spectrum asymptotes and break points where $\bar{\omega}_1$, $\bar{\omega}_2$, $\bar{\omega}_3$ are given in Table 1 ($\bar{\omega}_1 = |\bar{s}_1|$, $\bar{\omega}_2 = |\bar{s}_2|$, etc.).

$$\tilde{H}_o/\tilde{H}_i^{(N)} = 1 + s \sum_{i=1}^{N} \tau_i + s^2 \sum_{i>j}^{N,N} \left[1 - (a_i/a_j)^3 \right] \tau_i \tau_j + \ldots.$$

$$\ldots. + s^N \prod_{i=1}^{N} \left[1 - (a_i/a_{i-1})^3 \right] \tau_i \qquad (14)$$

where $a_o = \infty$. As expected, $\tilde{H}_i^{(N)}$ has N poles lying on the negative real axis of the s-plane.

III. CYLINDRICAL SHIELDS

The procedure of solving the problem of a multi-surface cylindrical shield where the external magnetic field is perpendicular to the axis of the shield follows exactly that of the spherical shield described in Section II. The other polarization where the external magnetic field is parallel to the axis of the shield is treated in Reference 2. From the geometry depicted in Figures 7a,d one can immediately write down

$$\begin{aligned} \Phi_1 &= -\tilde{H}_o \rho \cos\phi + \frac{A}{\rho}\cos\phi && \rho \geq b_1 \\ \Phi_2 &= B\rho \cos\phi + \frac{C}{\rho}\cos\phi && b_1 \geq \rho \geq b_2 \\ \Phi_3 &= D\rho \cos\phi && \rho \leq b_2 \end{aligned} \tag{15}$$

Applying at $\rho = b_1$ and $\rho = b_2$ the boundary conditions (Ref.1)

$$\begin{aligned} \frac{\partial}{\partial\rho}\Phi_1 &= \frac{\partial}{\partial\rho}\Phi_2 && \rho = b_1 \\ \frac{\partial}{\partial\rho}\Phi_2 &= \frac{\partial}{\partial\rho}\Phi_3 && \rho = b_2 \\ \nabla_s^2(\Phi_2 - \Phi_1) &= st_1 \frac{\partial}{\partial\rho}\Phi_1 && \rho = b_1 \\ \nabla_s^2(\Phi_3 - \Phi_2) &= st_2 \frac{\partial}{\partial\rho}\Phi_2 && \rho = b_2 \end{aligned} \tag{16}$$

to Equations 15 one gets

$$\frac{\tilde{H}_i(s)}{\tilde{H}_o(s)} = \frac{1}{(1+st_1)(1+st_2) - (b_2/b_1)^2 t_1 t_2 s^2} \tag{17}$$

where

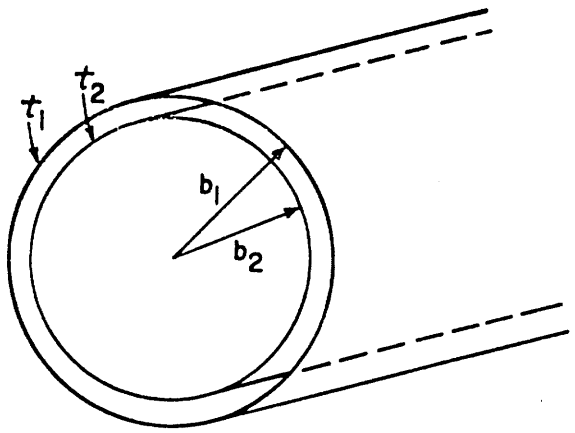

(a) Two-surface cylindrical shield

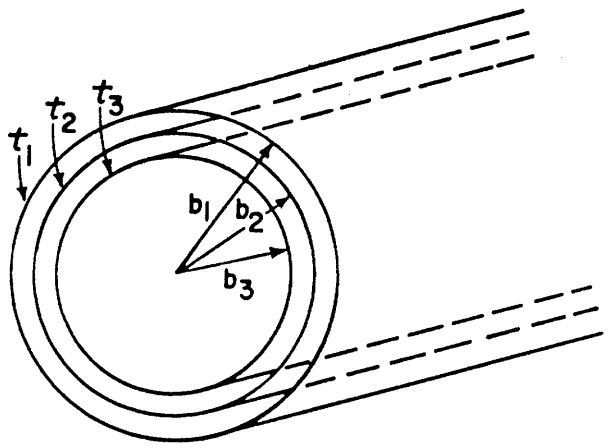

(b) Three-surface cylindrical shield

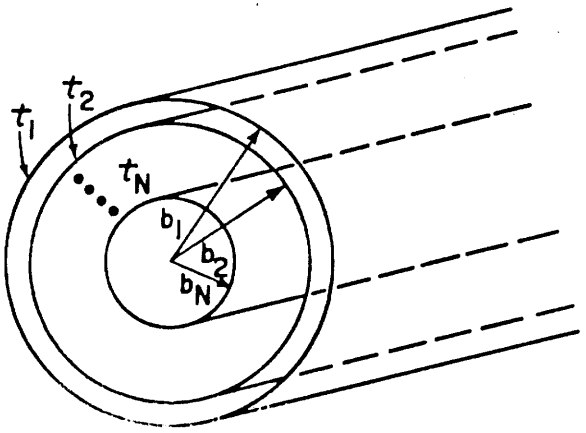

(c) N-surface cylindrical shield

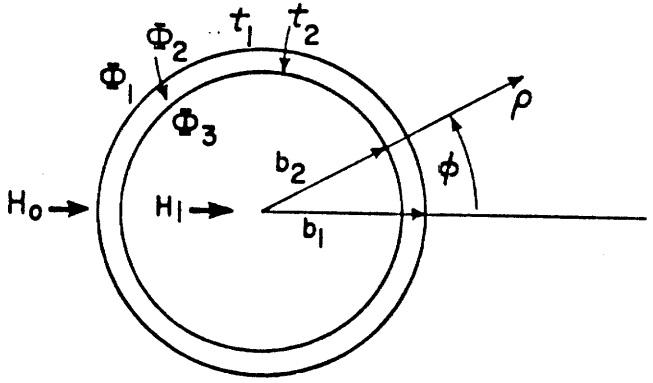

(d) Cross section of (a)

Figure 7. Multi-surface cylindrical shields.

$$t_1 = \frac{1}{2}\,\mu_o b_1 \sigma_1 \Delta_1$$

$$t_2 = \frac{1}{2}\,\mu_o b_2 \sigma_2 \Delta_2 \qquad (18)$$

Similarly, for a three-surface cylindrical shield (Fig. 7b) one has

$$\tilde{H}_o(s)/\tilde{H}_i^{(3)}(s) = 1 + (t_1+t_2+t_3)s + \left[1-(b_2/b_1)^2\right]t_1t_2s^2 + \left[1-(b_3/b_2)^2\right]t_2t_3s^2$$

$$+ \left[1-(b_3/b_1)^2\right]t_3t_1s^2 + \left[1-(b_2/b_1)^2\right]\left[1-(b_3/b_2)^2\right]t_1t_2t_3s^3 \qquad (19)$$

and for an N-surface cylindrical shield (Fig. 7c) one has

$$\tilde{H}_o(s)/\tilde{H}_i^{(N)}(s) = 1 + s\sum_{i=1}^{N} t_i + s^2 \sum_{i>j}^{N,N}\left[1-(b_i/b_j)^2\right]t_it_j + \ldots.$$

$$\ldots. + s^N \prod_{i=1}^{N}\left[1-(b_i/b_{i-1})^2\right]t_i \qquad (20)$$

where $b_o = \infty$. A comparison of Equations 17 through 20 with Equations 4, 5, 13 and 14 reveals that the results for spherical shields obtained in the last section can be directly used for cylindrical shields if one replaces

spherical shields		cylindrical shields
$(a_i/a_j)^3$	by	$(b_i/b_j)^2$
τ_i	by	t_i

Therefore, in the following two sections on equivalent-circuit representation and effects of bonding, discussions will be restricted only to the case of spherical shields.

Table 2 gives the s-plane poles for $\tilde{H}_i$ for two and three cylindrical shields, while Figure 8 shows the frequency spectrum asymptotes and break points for $|\tilde{H}_i/\tilde{H}_o|$.

TABLE 2. s-PLANE POLES FOR TWO-SURFACE AND THREE-SURFACE CYLINDRICAL SHIELDS. THE VALUES ARE FOR $\bar{s} = st_1$ WITH $\beta = b_2/b_1 = b_3/b_2$ AND $t_2/t_1 = t_3/t_2 = \beta$

β	Two Shields		Three Shields		
	$\bar{s}_1$	$\bar{s}_2$	$\bar{s}_1$	$\bar{s}_2$	$\bar{s}_3$
0.1	- 1.00	-10.11	- 1.00	-10.10	-101.12
0.2	- .99	- 5.26	- .99	- 5.21	- 26.30
0.3	- .96	- 3.80	- .96	- 3.66	- 12.68
0.4	- .92	- 3.25	- .91	- 2.98	- 8.20
0.5	- .85	- 3.15	- .82	- 2.67	- 6.51
0.6	- .77	- 3.40	- .71	- 2.60	- 6.13
0.7	- .69	- 4.07	- .59	- 2.80	- 6.74
0.8	- .62	- 5.63	- .49	- 3.47	- 8.85
0.9	- .55	-10.56	- .40	- 5.85	- 16.09

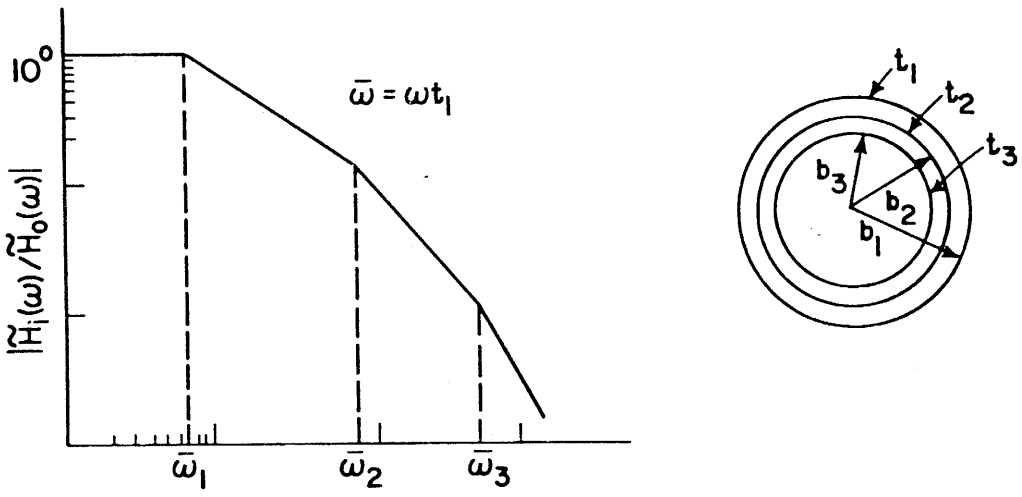

Figure 8. Frequency spectrum asymptotes and break points given in Table 2.

IV. EQUIVALENT CIRCUIT REPRESENTATION - GENERALIZATION TO SHIELDS OF ARBITRARY SHAPE

The results obtained in the last two sections will be interpreted in terms of equivalent circuits in this section. The advantages of equivalent circuit representation of mathematical results are two-fold: (1) it is useful for interpreting results and understanding physical mechanism involved, and (2) it is a quick way to generalize the results for specific shapes of enclosure to arbitrary shapes of enclosure.

To gain more familiarity with what follows one starts with one-surface spherical shielded enclosure (Fig. 9a) whose low-frequency transfer function is (Ref. 1)

$$\frac{\tilde{H}_i(s)}{\tilde{H}_o(s)} = \frac{1}{1+\tau s} \tag{21}$$

with

$$\tau = \frac{1}{3}\mu_o a\sigma\Delta \tag{22}$$

where μ_o, σ, a and Δ are defined in Figure 9a. Equation 21 can be represented by either the equivalent circuit of Figure 9b or Figure 9c where

$$L = \frac{1}{3}\mu_o a, \qquad R = \frac{1}{\sigma\Delta} \tag{23}$$

The inductance L can be expressed in terms of the volume V and the surface S of the enclosure as

$$L = \mu_o V/S \tag{24}$$

which also applies directly to cylindrical as well as two-parallel-plate enclosures (Ref.1). Equation 21 can thus be used as the transfer function of a single-surface shielded enclosure of arbitrary shape if τ is interpreted as

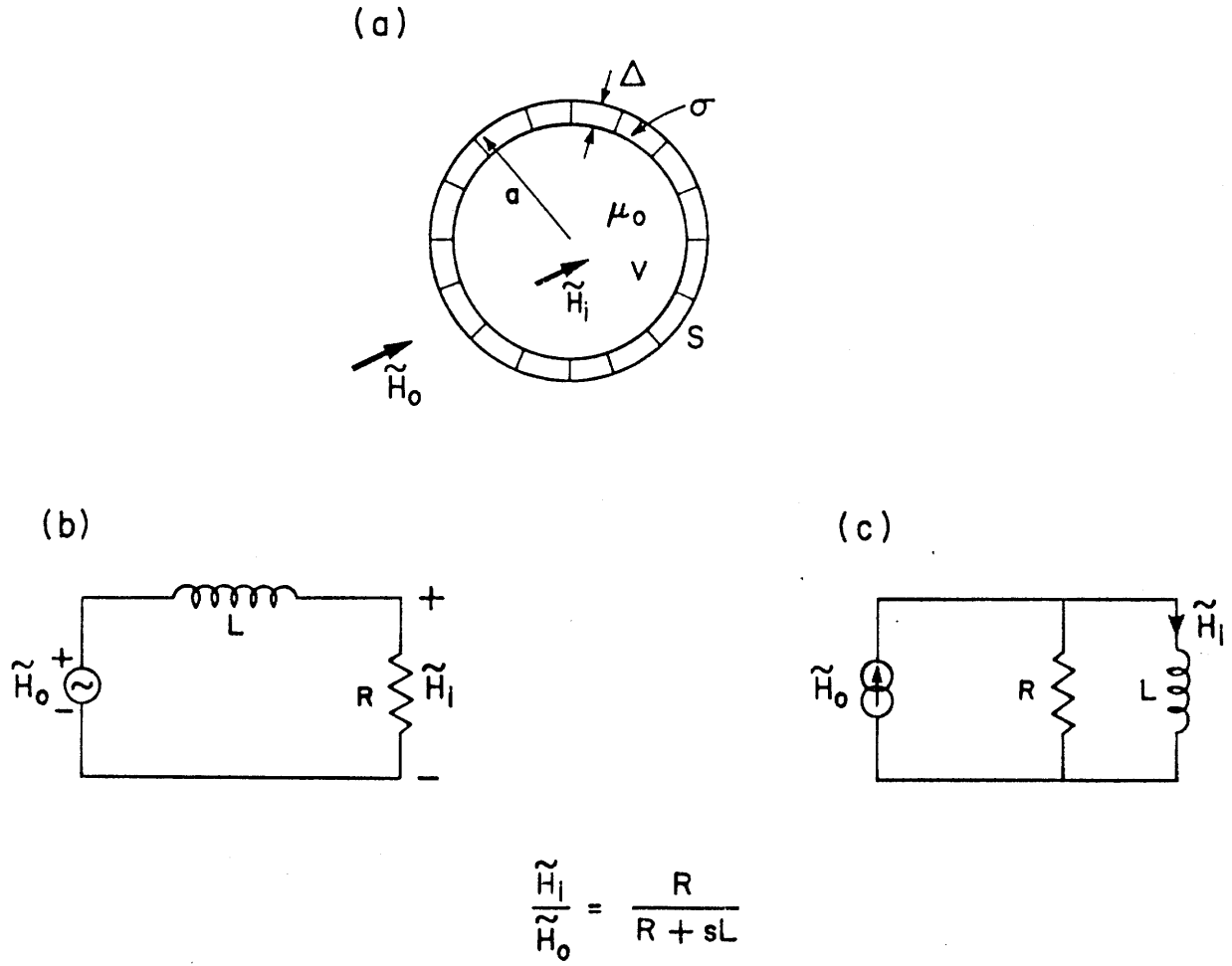

$$\frac{\tilde{H}_i}{\tilde{H}_0} = \frac{R}{R + sL}$$

Figure 9. Equivalent circuits of a spherical shield.

$$\tau = \frac{L}{R} \tag{25}$$

with L given by Equation 24 and R by $(\sigma\Delta)^{-1}$.

The extension of the equivalent circuit given in either Figure 9b or 9c for a single-surface enclosure to a two-surface enclosure turns out to be a nontrivial matter. In principle, one may start with the transfer function given in Equation 4 and constructs an equivalent circuit for it using the techniques known in circuit synthesis (Ref. 3). This approach, however, does not easily lead to a circuit which represents the actual physical phenomenon of the problem. To derive the desirable circuit one returns to the induced currents in the shields given by Equations 10 and 11. The total induced current in each shield is obtained by integrating Equations 10 and 11. Thus,

$$\tilde{I}_1 = \int_0^{\pi} \tilde{K}_{1\phi} a_1 d\theta = -3\tilde{H}_o a_1 \frac{\tau_1 s(1+\tau_2 s) - \alpha^3 \tau_1 \tau_2 s^2}{(1+\tau_1 s)(1+\tau_2 s) - (a_2/a_1)^3 \tau_1 \tau_2 s^2} \tag{26}$$

$$\tilde{I}_2 = \int_0^{\pi} \tilde{K}_{2\phi} a_2 d\theta = -3\tilde{H}_o a_2 \frac{\tau_2 s}{(1+\tau_1 s)(1+\tau_2 s) - \alpha^3 \tau_1 \tau_2 s^2} \tag{27}$$

To generalize Equations 26 and 27 to two-surface enclosures of arbitrary shape one simply sets

$$\tau_1 = \frac{L_1}{R_1}, \quad \tau_2 = \frac{L_2}{R_2}, \quad \alpha^3 \tau_1 \tau_2 = M^2/(R_1 R_2) \tag{28}$$

where the self-inductances L_1, L_2, the mutual inductance M, and the resistances R_1, R_2 are given by

$$L_1 = \frac{\mu_o V_1}{S_1}, \quad L_2 = \frac{\mu_o V_2}{S_2}, \quad M^2 = \frac{V_2}{V_1} L_1 L_2$$

$$R_1 = \frac{1}{\sigma_1 \Delta_1}, \qquad R_2 = \frac{1}{\sigma_2 \Delta_2} \tag{29}$$

Here, V_1 and V_2 are the volumes enclosed respectively by the surfaces S_1 and S_2 of the first and second shield. Equations 26 and 27 can be written in the general form

$$\tilde{I}_1 = \frac{sL_1(sL_2 + R_2) - s^2M^2}{(sL_1 + R_1)(sL_2 + R_2) - s^2M^2} \tilde{I}_o \tag{30}$$

$$\tilde{I}_2 = \frac{sMR_1}{(sL_1 + R_1)(sL_2 + R_2) - s^2M^2} \tilde{I}_o \tag{31}$$

with

$$\tilde{I}_o = - 3\tilde{H}_o a_1 \tag{32}$$

It can be easily verified that the equivalent circuit shown in Figure 10 leads to Equations 30 and 31.

It remains to show how $\tilde{I}_1$ and $\tilde{I}_2$ are related to the penetrant field $\tilde{H}_i$ given by Equation 4, which can be expressed in the generalized form

$$\frac{\tilde{H}_i}{\tilde{H}_o} = \frac{R_1R_2}{(sL_1 + R_1)(sL_2 + R_2) - s^2M^2} \tag{33}$$

From Equations 30 and 31 one gets

$$1 - \frac{1}{\tilde{I}_o}\left(\tilde{I}_1 + \frac{L_2}{M}\tilde{I}_2\right) = \frac{R_1R_2}{(sL_1 + R_1)(sL_2 + R_2) - s^2M^2} \tag{34}$$

The scaling factor L_2/M can be expressed in terms of the geometric parameters of the two shields with Equations 29 and is given by

$$\frac{L_2}{M} = \sqrt{\frac{S_1}{S_2}} \tag{35}$$

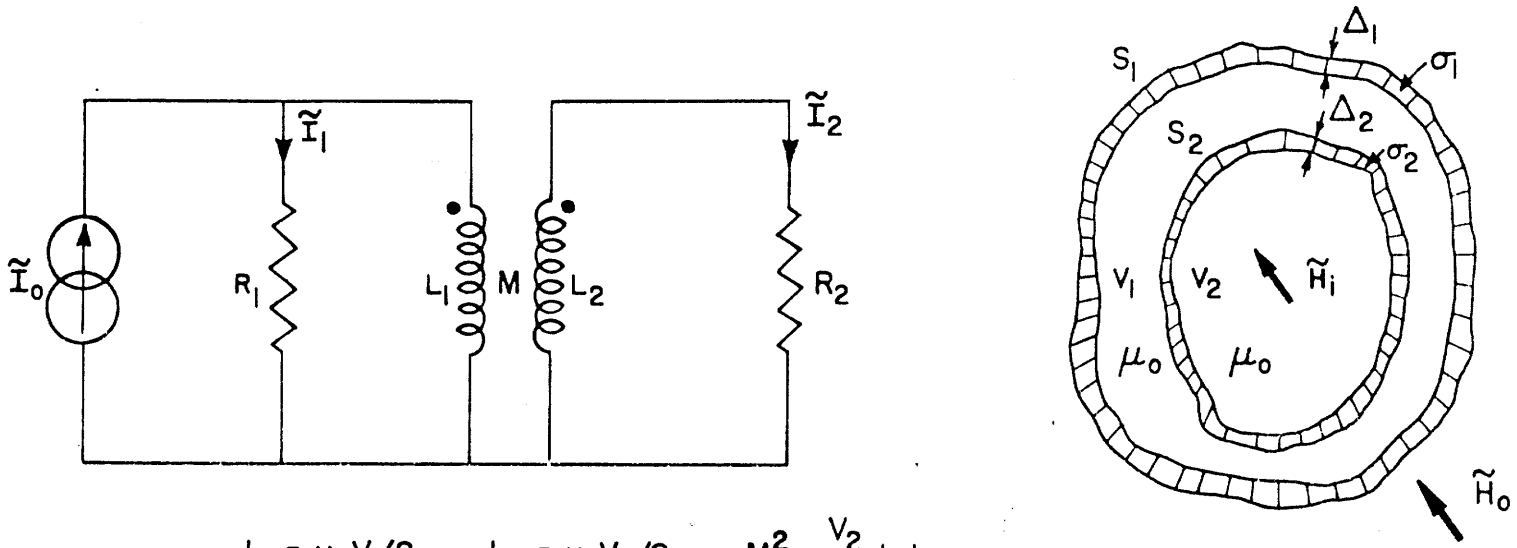

$$L_1 = \mu_0 V_1 / S_1 \qquad L_2 = \mu_0 V_2 / S_2 \qquad M^2 = \frac{V_2}{V_1} L_1 L_2$$

$$R_1 = \frac{1}{\sigma_1 \Delta_1} \qquad R_2 = \frac{1}{\sigma_2 \Delta_2} \qquad \frac{\tilde{H}_i}{\tilde{H}_0} = 1 - \frac{1}{\tilde{I}_0}\left(\tilde{I}_1 + \sqrt{\frac{S_1}{S_2}}\,\tilde{I}_2\right)$$

Figure 10. Equivalent circuit of two-surface enclosure.

Hence, one has on comparing Equations 33 and 34

$$\frac{\tilde{H}_i}{\tilde{H}_o} = 1 - \frac{1}{\tilde{I}_o}\left(\tilde{I}_1 + \sqrt{\frac{S_1}{S_2}}\,\tilde{I}_2\right) \tag{36}$$

which is to say, one can first calculate $\tilde{I}_1$ and $\tilde{I}_2$ from the equivalent circuit of Figure 10 from which the penetrant field $\tilde{H}_i$ is directly deduced from Equation 36.

A final point should be made about the scaling factor $\sqrt{S_1/S_2}$ in Equation 36. This factor comes about because the magnetic field $\tilde{H}$ is proportional to current density $\tilde{K}$ rather than the total current $\tilde{I}$.

V. TWO SPHERICAL SHIELDS OF ARBITRARY ELECTRICAL THICKNESS

In the previous sections the thickness of the shield's wall was assumed to be electrically thin. This assumption holds true for low frequencies and/or poorly conducting shields. In this section this assumption will be removed and the shield's wall can be of arbitrary electrical thickness.

As in Equation 1 let the scalar potential Φ for the three regions shown in Figure 2b take the form

$$\begin{aligned}
\Phi_1 &= -\tilde{H}_o r\cos\theta + A'\frac{a_1^3}{r^2}\cos\theta \qquad && r \geq a_1 \\
\Phi_2 &= B'r\cos\theta + C'\frac{a_1^3}{r^2}\cos\theta \qquad && a_1 \geq r \geq a_2 \\
\Phi_3 &= D'r\cos\theta \qquad && r \leq a_2
\end{aligned} \tag{37}$$

Instead of the boundary conditions given by Equations 2 and 3, the boundary conditions are now given by (Ref. 1)

$$\begin{aligned}
\frac{\partial}{\partial r}(\Phi_2 + \Phi_1) &= \alpha_1 \nabla_s^2(\Phi_2 - \Phi_1) \qquad \text{at } r = a_1 \\
\frac{\partial}{\partial r}(\Phi_2 - \Phi_1) &= \beta_1 \nabla_s^2(\Phi_2 + \Phi_1) \qquad \text{at } r = a_1
\end{aligned} \tag{38}$$

$$\begin{aligned}
\frac{\partial}{\partial r}(\Phi_3 + \Phi_2) &= \alpha_2 \nabla_s^2(\Phi_3 - \Phi_2) \qquad \text{at } r = a_2 \\
\frac{\partial}{\partial r}(\Phi_3 - \Phi_2) &= \beta_2 \nabla_s^2(\Phi_3 + \Phi_2) \qquad \text{at } r = a_2
\end{aligned} \tag{39}$$

where

$$\begin{aligned}
\alpha_i &= \frac{\mu_i \Delta_i}{\mu_o p_i}\frac{1}{\tanh(p_i/2)} \\
\beta_i &= \frac{\mu_i \Delta_i}{\mu_o p_i}\tanh(p_i/2) \\
p_i^2 &= s\mu_i \sigma_i \Delta_i^2
\end{aligned} \tag{40}$$

and $i = 1,2$. The constants A', B', C' and D' can be found by substituting Equation 37 into Equations 38, 39 and 40, and are given in Appendix A. The penetrant field $\tilde{H}_i$ is obtained from $-\nabla\Phi_3$ and given by

$$\frac{\tilde{H}_i}{\tilde{H}_o} = \frac{1}{(\cosh p_1 + K_1 p_1 \sinh p_i)(\cosh p_2 + K_2 p_2 \sinh p_2) - (a_2/a_1)^3 K_1 p_1 K_2 p_2 \sinh p_1 \sinh p_2} \tag{41}$$

with

$$K_1 = \frac{\mu_o a_1}{3\mu_1 \Delta_1}, \qquad K_2 = \frac{\mu_o a_2}{3\mu_2 \Delta_2} \tag{42}$$

Just like Equation 4 the combined transfer function of two shields is the reciprocal of the product of the transfer functions of individual shields minus an interaction term.

For electrical thin shield's walls (i.e., $p_1, p_2 << 1$), Equation 41 reduces to Equation 4, as it should. On the other hand, if the shield's walls are electrically thick (i.e., $p_1, p_2 >> 1$), then Equation 41 gives

$$\frac{\tilde{H}_i}{\tilde{H}_o} \sim \frac{4e^{-(p_1+p_2)}}{(1+K_1 p_1)(1+K_2 p_2) - (a_2/a_1)^3 K_1 p_1 K_2 p_2} \tag{43}$$

in which one may drop the ones in comparison with $K_1 p_1$ and $K_2 p_2$. However, Equation 43 is preferable since it is similar in form to Equation 4 for the case of an electrically thin shield.

Equation 43 is plotted in Figure 11 with and without the interaction term $(a_2/a_1)^3 K_1 p_1 K_2 p_2$. It can be concluded that for $a_2/a_1 = 0.9$ and $\omega\tau_2 > 100$ (which corresponds to $f > 16$ kHz for $\tau_2 \simeq 1$ ms), the shield-shield interaction reduces the shielding effectiveness by at least a factor of 3 or 10 dB.

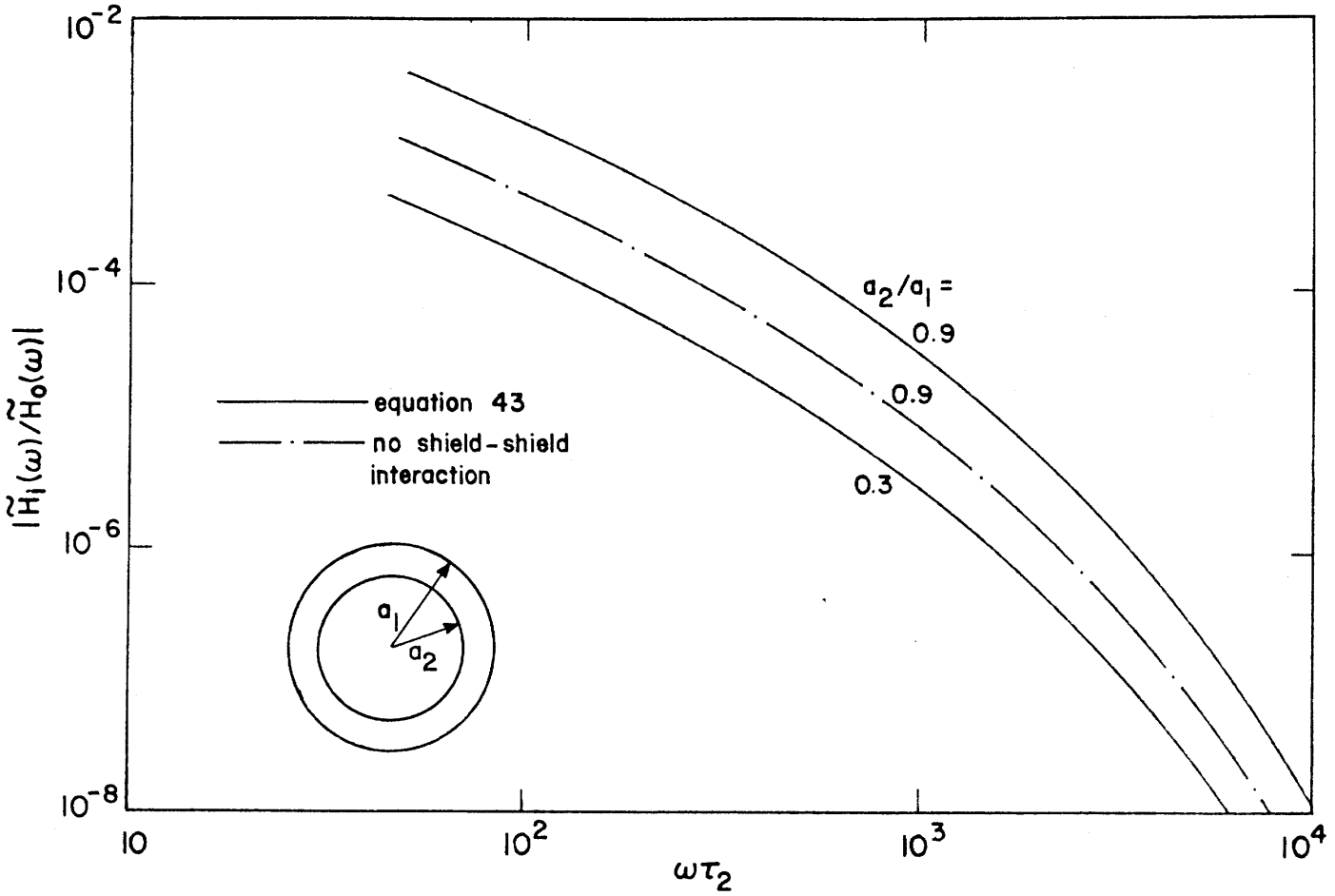

Figure 11. Frequency spectrum of the transfer function $|\tilde{H}_i/\tilde{H}_o|$ for two electrically thick spherical shields ($\Delta_1 = \Delta_2$, $\Delta_2/a_2 = \pi \times 10^{-3}$).

VI. EFFECT OF BONDING

Although bonding is often employed between shields in engineering practice to reduce electrostatic hazards, there is no quantitative information on its possible effect on the shielding performance of a shielded enclosure against the low-frequency magnetic-field penetration. This section is devoted to calculating this effect for two electrically-thin spherical shields.

In Figure 12 are shown various connection arrangements of bonding straps between the two surfaces of a spherical enclosure. Later in this section it will become clear that the bonding strap arrangements (a) through (d) have no effect on the magnetic-field shielding performance of the enclosure, while the arrangement (e) has a significant adverse effect. Before proceeding it is appropriate to remark that the low-frequency electric field within a conducting enclosure comes mainly from the eddy currents in the enclosure's wall induced by the time rate of change of the external magnetic field. It is this electric field that is affected by the bonding straps in the inductive shielding approximation.

Return now to Figure 12e (which is redrawn in Figure 13) and calculate the current induced in the bonding straps. Let the unprimed quantities be the quantities in the absence of the bonding straps, and the primed quantities the quantities due to the presence of the bonding straps. Then, integrating the equation

$$\nabla \times \vec{E} = - s\mu_o \vec{H} \tag{44}$$

over the area enclosed and traced out counter clockwise by the loop BCDAB of Figure 13, one gets

$$V_{BC} + V'_{BC} - V_{AD} - V'_{AD} = s\Psi_{ABCDA} + s\Psi'_{ABCDA} \tag{45}$$

where V is the voltage drop and ψ is the magnetic flux. In deriving Equation 45 the bonding straps have been assumed to be good conductors; otherwise, a term for the voltage drop along AB and CD has to be added to the left hand side of the equation.

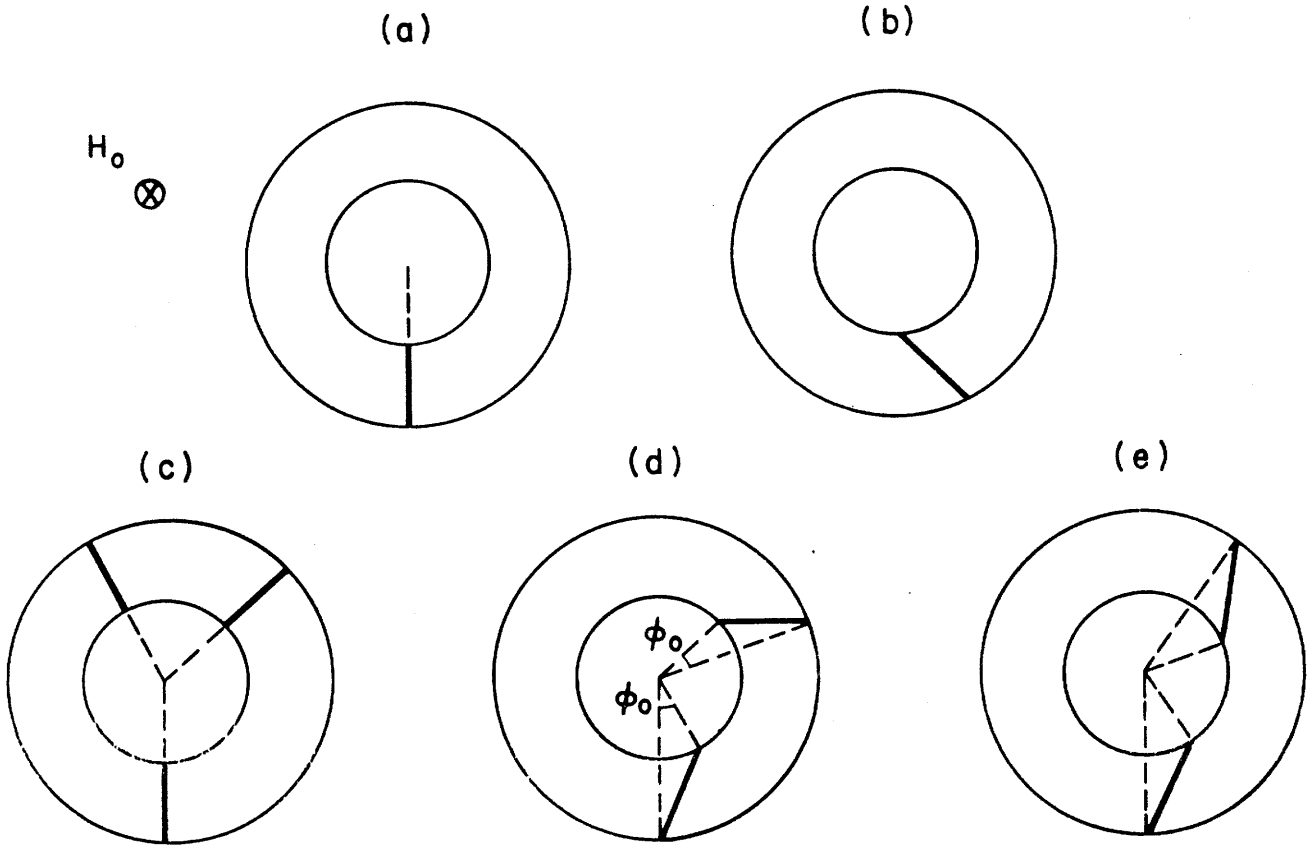

Figure 12. Different arrangements of conducting straps bonding two spherical shields.

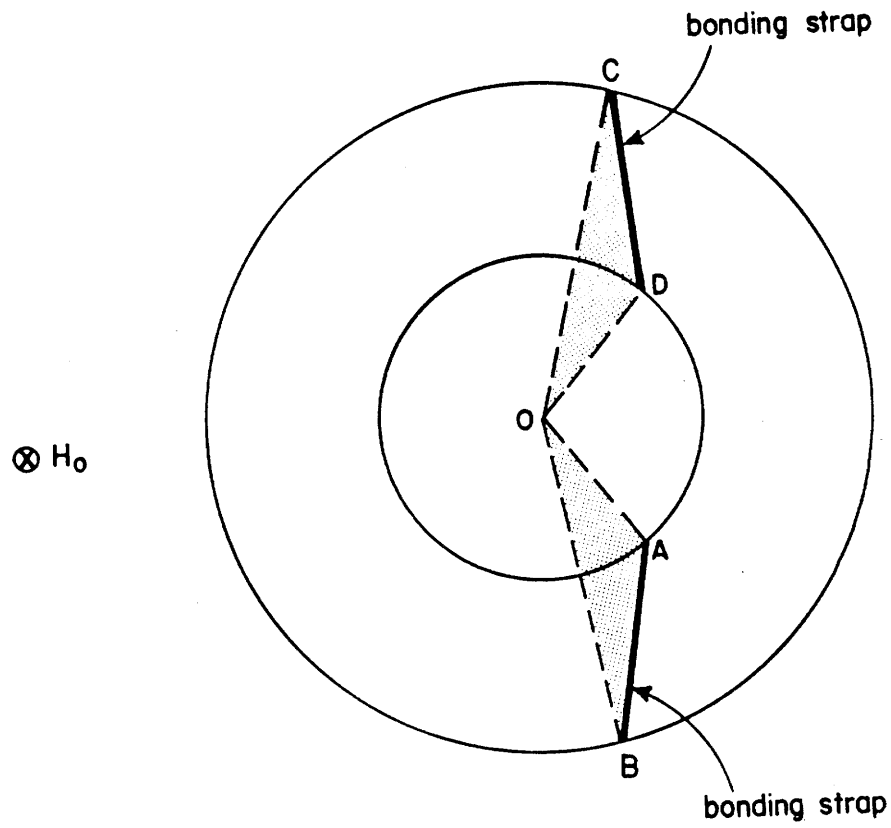

Figure 13. A two-spherical shield enclosure with two bonding straps lying in the equatorial plane perpendicular to the external magnetic field H_o.

Let $\tilde{I}_b$ = current in bonding strap, L_b = inductance of one bonding strap, R_{BC} or R_{DA} = resistance between B,C of the outer shield, or D,A of the inner shield. It is obvious from Equation 44 that

$$\begin{aligned}\tilde{I}_b(R_{BC}+R_{DA}+2sL_b) &= s\Psi_{ABCDA} - V_{BC} + V_{AD} \\ &= s\Psi_{ABCDA} - s\Psi_{OBCO} + s\Psi_{OADO} \\ &= -s(\Psi_{OAB} + \Psi_{OCD}) \\ &= -2s\Psi_{OAB}\end{aligned} \tag{46}$$

The second step of the right hand side follows from repeated applications of Equation 44. It has been assumed for simplicity that the two bonding straps are identical. Hence, the triangle OAB is equivalent to the triangle OCD.

Similarly, an application of Equation 44 to the area enclosed by the loop BADCB going counter clockwise in Figure 13 gives Equation 46, as it should.

Solving Equation 46 for $\tilde{I}_b$ and using the expression in Appendix B for Ψ_{OAB} one obtains

$$\begin{aligned}\tilde{I}_b &= \frac{-2s\Psi_{OAB}}{R_{BC}+R_{DA}+2sL_b} \\ &= -\frac{F\tilde{H}_o}{R_s}\,\frac{s(1+sT_o)}{(1+sT_b)(1+sT_1)(1+sT_2)}\end{aligned} \tag{47}$$

where $R_s = R_{BC} + R_{DA}$, $T_b = 2L_b/R_s$, T_1 and T_2 are given in Equation 8, F and T_o are given in Appendix B. It can be shown that for practical cases T_o is small compared to the decay time constant τ_2 of the inner shield. Hence for low frequencies one may use the approximation

$$\frac{\tilde{I}_b}{\tilde{V}_o/R_s} \simeq -\frac{s\tau_2}{(1+sT_b)(1+sT_1)(1+sT_2)} \tag{48}$$

with $\tilde{V}_o = F\tilde{H}_o/\tau_2$, where $F\tilde{H}_o$ is identically equal to the external magnetic flux linking the two triangles shown in Figure 13.

The magnitude of Equation 48 is plotted in Figure 14 against $\omega\tau_2$ with T_b/τ_2 as a parameter. The time histories of I_b and $\dot{I}_b$ are shown in Figures 15 and 16 for an impulsive external magnetic field $H_o\delta(t)$, which is a valid representation of any pulsed external field whose pulse width is less than the diffusion time through the shield's wall. The diffusion time of a typical metallic enclosure is on the order of tens of microseconds. The parameter T_b/τ_2 is roughly equal to the ratio of the inductance of the two bonding straps to the inductance of the inner enclosure, the latter being given by $\mu_o a_2/3$; that is to say

$$\frac{T_b}{\tau_2} \simeq \frac{2L_b}{L_2} = \frac{6L_b}{\mu_o a_2} \tag{49}$$

where L_b can be estimated from the approximate formula

$$L_b \simeq \frac{\mu_o \ell}{2\pi} \ell n(\ell/r) \tag{50}$$

with ℓ = length of one bonding strap, r = effective cross-sectional radius of the strap. It can be seen from Equations 49 and 50 that T_b/τ_2 is usually less than unity. The smaller is this parameter the more current will be induced in the bonding straps, as can be observed in Figures 14 through 16. Of course, the more current there is in the bonding straps the more penetration there is into the enclosure. Table 3 summarizes the peak values for $I_b(t)$ and $\dot{I}_b(t)$ for various values of T_b/τ_2. In the table it is assumed that $a_2/a_1 = 0.9$, $R_s \simeq (\sigma\Delta)^{-1}$, and the two shields have the same thickness, conductivity and permeability.

To get some rough estimate on the field due to the bonding strap current I_b one may divide I_b by $2\pi a_2$. From Table 3 and for the case $T_b/\tau_2 = 0.01$ the peak penetrant fields due to I_b are

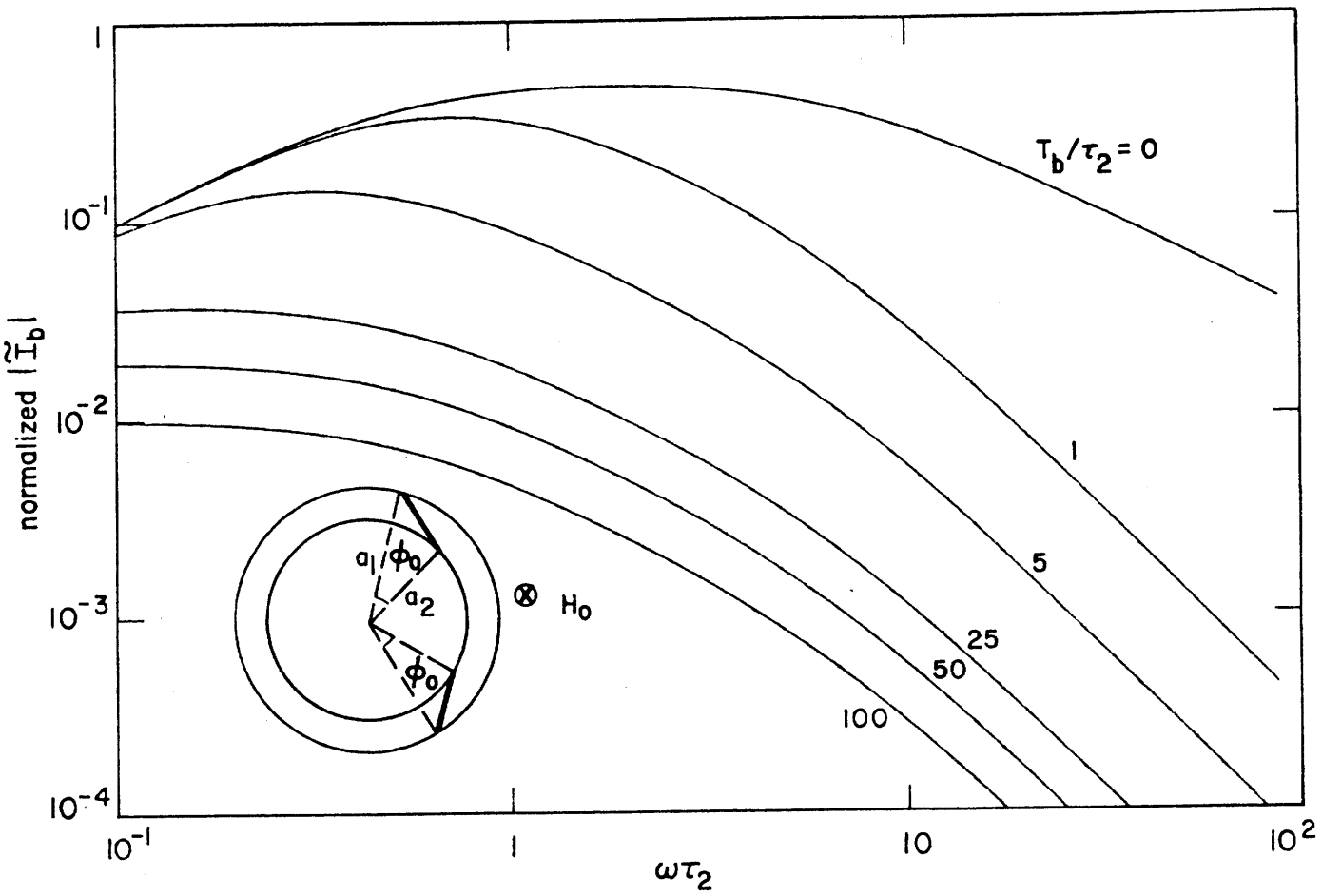

Figure 14. Frequency spectrum of the bonding strap current. The normalizing factor is $\tilde{V}_o/R_s$, where $\tilde{V}_o = F\tilde{H}_o/\tau_2$. $F\tilde{H}_o$ is equal to the flux linking the two triangles by the external field.

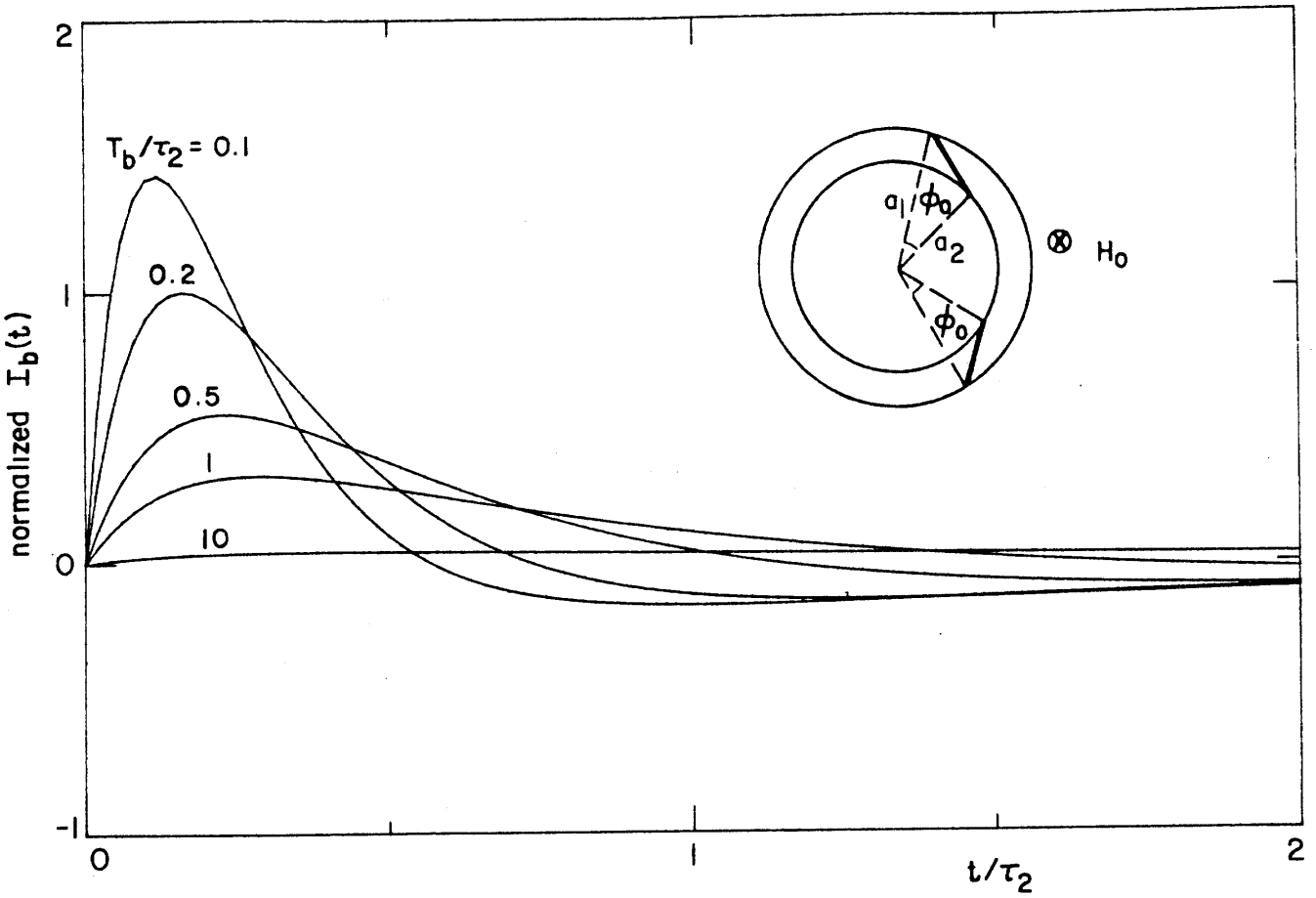

Figure 15. Time behavior of the bonding strap current due to an impulsive external magnetic field $H_o\delta(t)$. The normalizing factor is V_o/R_s with $V_o = FH_o/\tau_2^2$. Note that H_o has the dimension of ampere-second.

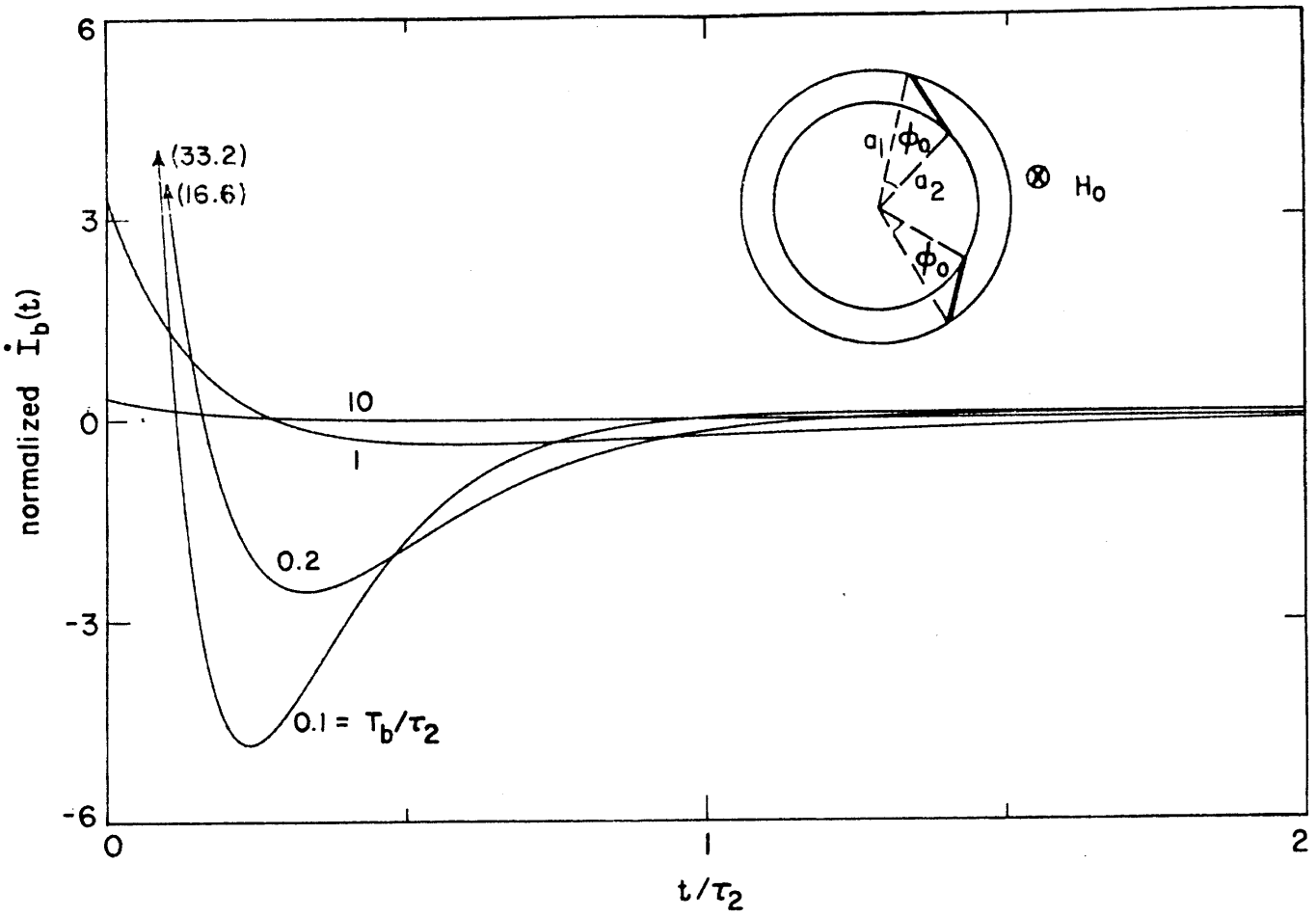

Figure 16. Time behavior of the time rate of change of the bonding strap current due to an impulsive external field $H_o\delta(t)$. The normalizing factor is $V_o/R_s\tau_2$. The numbers in parenthesis indicate the values the curves intercept the ordinate axis.

TABLE 3. PEAK VALUES FOR I_b AND $\dot{I}_b$

T_b/τ_2	0.01	0.1	0.2	0.5	1	≥ 5
$\frac{\tau_2 I_b(\text{peak})}{H_o a_2 \sin\phi_o}$	3.1	1.57	1.11	0.61	0.36	$\frac{0.43\ \tau_2}{T_b}$
$\frac{\tau_2^2 \dot{I}_b(\text{peak})}{H_o a_2 \sin\phi_o}$	370	37.0	19.0	7.4	3.7	$\frac{3.7\ \tau_2}{T_b}$

$$H_i^{(1)}(\text{peak}) \simeq \frac{1}{2\tau_2} H_o \sin\phi_o$$

$$\dot{H}_i^{(1)}(\text{peak}) \simeq \frac{60}{\tau_2^2} H_o \sin\phi_o \qquad (51)$$

That part due to direct field penetration can be read off from Figure 4 for $a_2/a_1 = 0.9$ and is given by

$$H_i^{(0)}(\text{peak}) \simeq \frac{0.4}{\tau_2} H_o$$

$$\dot{H}_i^{(0)}(\text{peak}) \simeq \frac{3.5}{\tau_2^2} H_o \qquad (52)$$

The total peak penetrant fields, $H_i(\text{peak})$ and $\dot{H}_i(\text{peak})$, with bonding straps are the sum of Equations 51 and 52. It can be seen that the bonding straps will increase $H_i(\text{peak})$ by a factor of two and $\dot{H}_i(\text{peak})$ by as much as an order of magnitude.

VII. CONCLUSIONS

It is found that the inductive interactions among the shields and the presence of conducting straps bonding the shields reduce the effectiveness of a multi-surface shielded enclosure against the penetration of external magnetic fields.

For a two-surface spherical shielded enclosure the important findings can be summarized as follows. Let

$H_{i,p}$ = peak interior (penetrant) field

$\dot{H}_{i,p}$ = peak time rate of change of $H_i(t)$ = peak electromotance force (emf) density

$|\tilde{H}_i|$ = frequency spectrum of $H_i(t)$

and let the ratio of radii of inner to outer shield = 0.9.

1. Neglect of interaction of electrically thin shields under-estimates
   - $H_{i,p}$ by 20%
   - $\dot{H}_{i,p}$ by a factor of 4
   - $|\tilde{H}_i|$ by one order of magnitude for f > 100 kHz and enclosures with L/R time constant ≃ 100 μs.
2. Neglect of interaction of electrically thick shields under-estimates
   - $|\tilde{H}_i|$ by a factor of 3 for f > 160 kHz and enclosures with L/R time constant ≃ 100 μs.
3. Two bonding straps, each subtending a 22.5° angle at the center and with inductance $2L_b = 0.01\ L_2$ ($L_2 \simeq 0.2$ μH for an enclosure of one-meter diameter), increase
   - $H_{i,p}$ by a factor of 2
   - $\dot{H}_{i,p}$ by one order of magnitude

REFERENCES

[1] Lee, K.S.H., ed., EMP Interaction: Principles, Techniques and Reference Data, (A Compleat Concatenation of Technology From The EMP Interaction Notes), EMP Interaction 2-1, December 1980.

[2] Baum, C.E., "Conducting Shields for Electrically Small Cylindrical Loops," Sensor and Simulation Notes, Note 40, May 1967.

[3] Guillemin, E.A., Synthesis of Passive Networks, John Wiley & Sons, Inc., New York, 1957.

APPENDIX A

THE CONSTANTS

The constants A, B, C and D that appear in Equation 1 are given by

$$A = -\frac{\tilde{H}_o}{2}\ \frac{s(\tau_1+\alpha^3\tau_2) + s^2\tau_1\tau_2(1-\alpha^3)}{(1+s\tau_1)(1+s\tau_2) - s^2\tau_1\tau_2\alpha^3}$$

$$B = -\tilde{H}_o\ \frac{1+s\tau_2}{(1+s\tau_1)(1+s\tau_2) - s^2\tau_1\tau_2\alpha^3}$$

$$C = -\frac{\tilde{H}_o}{2}\ \frac{s\tau_2\alpha^3}{(1+s\tau_1)(1+s\tau_2) - s^2\tau_1\tau_2\alpha^3}$$

$$D = -\tilde{H}_o\ \frac{1}{(1+s\tau_1)(1+s\tau_2) - s^2\tau_1\tau_2\alpha^3}$$

where $\alpha = a_2/a_1$, $\tau_1 = \mu_o a_1\sigma_1\Delta_1/3$, $\tau_2 = \mu_o a_2\sigma_2\Delta_2/3$.

The constants A', B', C' and D' that appear in Equation 37 are given by

$$A' = -\frac{\tilde{H}_o}{2F}\left\{\left(K_1p_1 - \frac{4}{9K_1p_1}\right)\sinh p_1\left[\cosh p_2 + \left(K_2p_2 + \frac{2}{9K_2p_2}\right)\sinh p_2\right] + \right.$$

$$\left. + \left(\frac{a_2}{a_1}\right)^3\left(K_2p_2 - \frac{4}{9K_2p_2}\right)\sinh p_2\left[\cosh p_1 - \left(K_1p_1 + \frac{2}{9K_1p_1}\right)\sinh p_1\right]\right\}$$

$$B' = -\frac{\tilde{H}_o}{F}\left[\cosh p_2 + \left(K_2p_2 + \frac{2}{9K_2p_2}\right)\sinh p_2\right]$$

$$C' = -\frac{\tilde{H}_o}{2F}\left(\frac{a_2}{a_1}\right)^3\left(K_2p_2 - \frac{4}{9K_2p_2}\right)\sinh p_2$$

$$D' = -\tilde{H}_o/F$$

where

$$p_1 = s\mu_1\sigma_1\Delta_1^2, \qquad p_2 = s\mu_2\sigma_2\Delta_2^2$$

$$K_1 = \frac{\mu_o a_1}{3\mu_1\Delta_1}, \qquad K_2 = \frac{\mu_o a_2}{3\mu_2\Delta_2}$$

$$F = \left[\cosh p_1 + \left(K_1p_1 + \frac{2}{9K_1p_1}\right)\sinh p_1\right]\left[\cosh p_2 + \left(K_2p_2 + \frac{2}{9K_2p_2}\right)\sinh p_2\right] -$$

$$- \left(\frac{a_2}{a_1}\right)^3\left(\frac{1}{9K_1p_1} - K_1p_1\right)\left(\frac{4}{9K_2p_2} - K_2p_2\right)\sinh p_1 \sinh p_2$$

Unless K_1 and K_2 are much smaller than unity one may neglect terms involving the reciprocal of K_1p_1 and K_2p_2 and obtains for F the following accurate expression

$$F \simeq (\cosh p_1 + K_1p_1\sinh p_1)(\cosh p_2 + K_2p_2\sinh p_2) -$$

$$- (a_2/a_1)^3 K_1p_1K_2p_2\sinh p_1\sinh p_2$$

APPENDIX B

CALCULATION OF ψ_{OAB}

The magnetic field at the equatorial plane ($\theta = \pi/2$) can be found from Equation 1, namely,

$$\tilde{H}_\theta = B + C\, a_1^3/r^3, \qquad a_2 < r < a_1$$
$$= D \qquad a_2 > r$$

The magnetic flux ψ_{OAB} can then be calculated via (Fig. B1)

$$\psi_{OAB} = -\mu_o \iint_{OAB} \tilde{H}_\theta dS$$

$$= -\mu_o \left\{ \frac{a_2^2 \phi_o}{2} D + \int_{a_2}^{a_1} \int_0^{\phi'} \left(B + C\, \frac{a_1^3}{r^3} \right) r d\phi dr \right\}$$

$$= -\mu_o \left\{ \frac{a_2^2 \phi_o}{2} D + \int_{a_2}^{a_1} \left[\sin^{-1}\left(\frac{a_1 \sin\gamma}{r} \right) - \gamma \right] \left(B + C\, \frac{a_1^3}{r^3} \right) r dr \right\}$$

$$= -\mu_o \left\{ \frac{a_2^2 \phi_o}{2} D + B \left[\frac{a_1 a_2}{2} \sin\phi_o - \frac{a_2^2}{2} \phi_o \right] \right.$$
$$\left. + C\, a_1^3 \left[\frac{\phi_o}{a_2} - \frac{\cos\gamma - \cos(\gamma + \phi_o)}{a_1 \sin\gamma} \right] \right\}$$

$$= \frac{1 + sT_o}{(1 + s\tau_1)(1 + s\tau_2) - \alpha^3 s^2 \tau_1 \tau_2} \frac{F\tilde{H}_o}{2}$$

where

$$F = \mu_o a_1 a_2 \sin\phi_o$$

$$T_o = \tau_2 \left[(1 - \alpha) + \alpha \tan(\phi_o/2)(\cos\phi_o - \alpha)/\sin\phi_o \right]$$

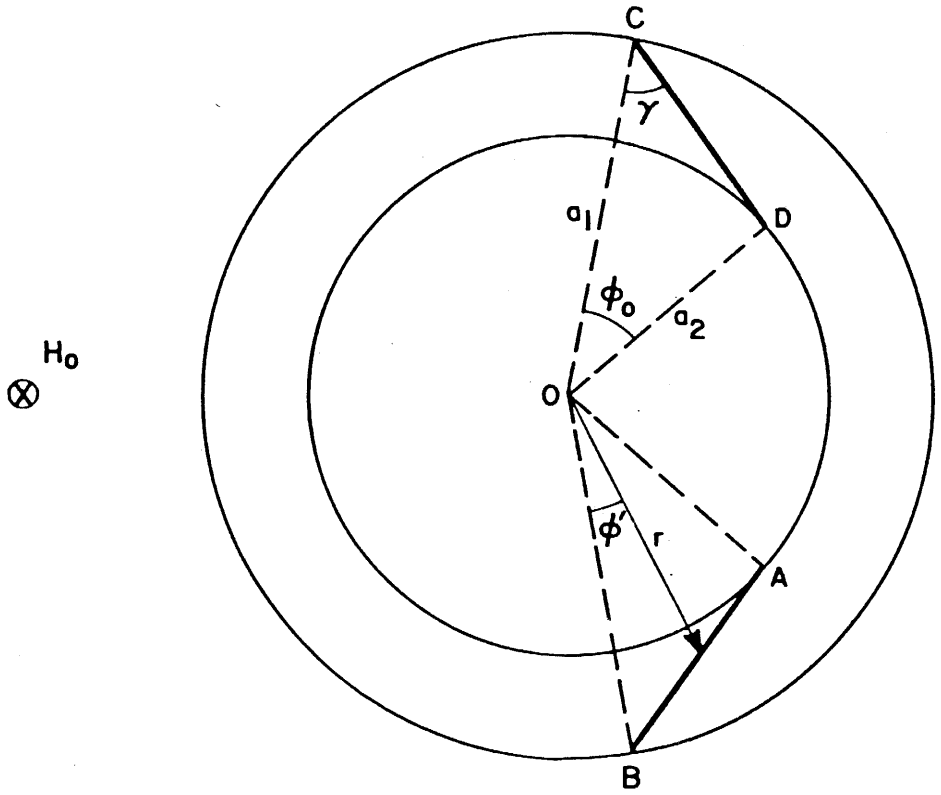

Figure B1. Geometry for calculating the flux ψ_{OAB}.